THE JOURNAL OF PHYSICAL CHEMISTRY B

pubs.acs.org/JPCB Article

Structural Changes in Liquid Lithium under High Pressure

Yu Shu, Yoshio Kono, Itaru Ohira, Rostislav Hrubiak, Curtis Kenney-Benson, Maddury Somayazulu, Nenad Velisavljevic, and Guoyin Shen*

Cite This: J. Phys. Chem. B 2020, 124, 7258−7262

Read Online

ACCESS | Metrics & More | Article Recommendations | Supporting Information

ABSTRACT: We have experimentally studied the effect of compression on the structure of liquid lithium (Li) by multiangle energy dispersive X-ray diffraction in a large-volume cupped-Drickamer-Toroidal cell. The structure factors, $s(q)$, of liquid Li have been successfully determined under an isothermal compression at 600 ± 30 K and at pressures up to 11.5 GPa. The first peak position in $s(q)$ is found to increase with increasing pressure and is showing an obvious slope change starting at ∼7.5 GPa. The slope change is interpreted as a structural change from bcc-like to fcc-like local ordering in liquid Li. At pressures above 8.7 GPa, the liquid Li becomes predominantly fcc-like up to the highest pressure of 11.5 GPa in this study. The observed structural changes in liquid Li are consistent with the recently determined melting curve of Li.

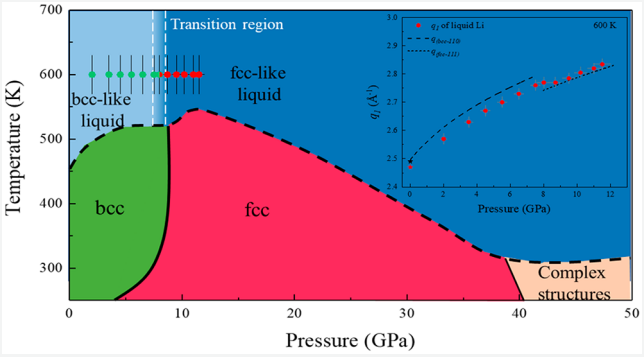

1. INTRODUCTION

Lithium (Li) is the lightest metallic element and often regarded as a prototype of simple metals with a body-centered cubic (bcc-Li) structure at ambient pressure and room-temperature conditions. Under high pressures, Li undergoes a series of transformations.[1−7] A transformation from the bcc-Li to a face-centered cubic (fcc-Li) phase occurs at 7.5 GPa at 298 K.[1] Subsequent transformations to the low-symmetry *h*R1 and *c*I16 structures are reported at 39 and 42 GPa, respectively, at 180 K.[3] With further compression, Li adopts a variety of complex structures (*oC88*, *oC40*, and *oC24*) up to 120 GPa at low temperatures.[5] These symmetry-breaking phase transitions are accompanied by changes in electronic structure and physical properties, including electron localization,[2−4,8] superconductivity,[9,10] and metal−semiconductor transitions.[6,7] Similar complex, pressure-induced, symmetry-breaking structural transitions and electronic localizations are also observed in other alkali metals.[11−16]

The melting curve of Li shows a complex behavior.[17−21] The melting temperature of bcc-Li first increases with increasing pressure up to ∼7 GPa. Then the melting curve of bcc-Li becomes nearly pressure independent at pressures of 7−9 GPa. Above 9 GPa in the stability field of fcc-Li, its melting curve displays a strong positive slope first and then a turnover to a negative slope up to 40 GPa. At higher pressures, the melting curve is observed to turnover again to a positive slope in the stability fields of phases with more complex structures.[18−20] It is interesting to note that the slope of the melting curve can change or even turn over within the stability field of a single solid phase. Considering that a liquid may exhibit different local orderings,[22,23] the slope changes in the melting curve may suggest possible structural changes in liquid Li under high pressure. Indeed, the experimental studies on other alkali liquids, such as K,[24] Rb,[25,26] and Cs,[27−29] show that the structural changes in liquid metals are largely responsible for the slope changes in the melting curves. For liquid Li so far, there are no experimental data reported on the liquid structure at high pressures. Molecular dynamics simulations predicted that liquid Li[30,31] would undergo structural changes from bcc-like to fcc-like and further to low-symmetry structured liquids under compression. However, very limited information is provided at pressures below 10 GPa from these simulation studies.

Major challenges in experimentally determining the structure of liquid Li include the weak signals in X-ray scattering and its inherent chemical reactivity. The structure of liquid Li has only been measured at ambient pressure.[32,33] We overcome the experimental difficulties by using a large volume high-pressure device to enhance the scattering intensity and by carefully selecting a capsule material to avoid any chemical reactions. We have successfully measured the structure of liquid Li under an isothermal compression path covering a pressure range from 2 to 11.5 GPa at a temperature of 600 ± 30 K by using a LiF cylindrical capsule.

Received: June 11, 2020
Revised: July 17, 2020
Published: July 21, 2020

https://dx.doi.org/10.1021/acs.jpcb.0c05324
J. Phys. Chem. B 2020, 124, 7258−7262

2. EXPERIMENTAL METHODS

The large volume pressure device is the Cupped-Drickamer-Toroidal (CDT) cell which can be combined with the multiangle energy dispersive X-ray diffraction technique for liquid structure determination.[34] As shown in Figure 1, a ring-shaped gasket (boron/epoxy = 4:1 in weight ratio) was used together with a supporting outer polycarbonate plastic (Lexan) ring and ZrO_2 caps. The boron-epoxy gasket and the ZrO_2 caps in the assembly provided good thermal insulation. The inner space of the gasket was filled with an MgO ring and a TiB_2 heater. High temperature was generated resistively by supplying a high current from the WC anvils through the Mo foil to the TiB_2 heater. A calibrated temperature-power curve is used to estimate the temperature in the measurements. We have tested several materials for encapsulating the reactive Li sample, such as hexagonal BN (h-BN), Teflon, cubic BN with epoxy (BN/epoxy = 10:1 in weight ratio) (c-BN), and LiF. Both h-BN and Teflon reacted quickly with the liquid Li sample even at very low pressure (~1 GPa). The c-BN capsule appeared stable in the experiments below 7 GPa and at temperatures lower than 600 K. However, above ~8 GPa, new crystalline diffraction peaks appeared in the spectrum, and the intensity of these peaks gradually increased over time, indicating that the c-BN capsule also gradually reacted with liquid Li at high pressures. We find that only a LiF capsule can maintain chemical stability in the pressure−temperature conditions of this study. No signs of chemical reactions are noticeable with no extra diffraction peaks other than those from crystalline LiF present during the measurements. Therefore, we chose LiF as a capsule material in this study. A Li grain (Alfa Aesar, 99%) was packed in a LiF capsule in a glovebox. The initial sample size was ~1 mm in diameter and 1 mm in thickness. The large sample volume is conducive to improve the signal-to-noise ratio. Both the MgO ring and LiF capsule are also used as pressure standards by using their equations of state.[35,36] We measured pressures from MgO and LiF before and after the structure measurement at each pressure point (~3.5 h for data collection) with a typical pressure difference of ~0.2−0.5 GPa. Here we use the average pressures from LiF measured before and after each pressure point in the structure measurements.

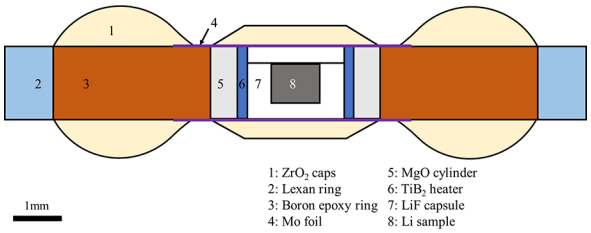

Figure 1. Schematic illustration of the Cupped-Drickamer-Toroidal (CDT) cell assembly for the measurements of the structure of liquid Li at high pressures. Compression loading is applied vertically, while the X-ray beam and the diffraction geometry are in the horizontal plane.

We used the energy dispersive X-ray diffraction (EDXD) technique in horizontal geometry for measuring X-ray scattering of liquid Li. In EDXD, for a given diffraction angle a pair of defining slits in front of the detector allow us to spatially resolve the weakly scattering sample from the surrounding material. In order to optimize the collimation for improved signal-to-background ratios, we used a Pt-coated silicon Kirkpatrick-Baez mirror with a length of 200 mm to focus the incident polychromatic, white X-rays down to 0.010 mm (full width at half-maximum) in the horizontal direction. We collected EDXD patterns at a series of 2θ angles (4.13°, 5.13°, 6.64°, 8.14°, 9.14°, 10.64°, 12.14°, 14.14°, 16.14°, 18.15°, 20.15°) using a Ge solid-state detector (Canberra). As shown in Figure S1a, the EDXD patterns are collected in a wide energy range from 0 to ~120 keV. However, in order to avoid the distinct oscillatory features at low energies and to reject instrument-induced systematic errors in the high energy range,[34] we only use the data between 35 and 58 keV in this study (see the detailed procedures in the Supporting Information). In addition to the scattering from liquid Li, several sharp peaks are superimposed in the raw data. The reason for the overlap is mainly related to the focused horizontal beam that has a typical Gaussian distribution in intensity. The tail size, for example, the full width at 1% maximum intensity is wider than 0.05 mm. This wide tail substantially increases the collimation depth, which results in the scattering intensities from surrounding materials (LiF and TiB_2) being included in our raw data, particularly at low angle. Because of the extremely weak signals from liquid Li, the background signals from the surrounding materials may not be completely eliminated. Fortunately, these residual diffraction peaks from the crystalline materials are sharp, compared to the broad features from liquid Li. We can remove these crystalline peaks by using the spline interpolation method (Figure S1b). It is noted that within the pressure range of this study the first peak of liquid Li does not overlap with any crystalline peaks (Figure S1c). However, the diffraction peak of LiF (220) superimposes on the second peak of liquid Li (Figure S1d). This overlap causes uncertainties in determining the second peak of $s(q)$ affected by the removal process of the crystalline peak. In addition, in the data collected at high angles, two unknown weak peaks appear at energies around 35 and 49 keV, respectively (Figure S1e). Their positions do not change with the 2θ diffraction angle, suggesting that they may be a background signal in the experimental setup. We also removed these two peaks using the spline interpolation method in the data analysis. After removing the sharp peaks, we applied a normalization procedure for structure factors of liquid Li using the aEDXD program developed based on the analysis theory of energy dispersive X-ray diffraction.[34,37,38] Further details of the data analysis procedures are given in the Supporting Information.

3. RESULTS AND DISCUSSION

As shown in Figure 2, the overall feature of $s(q)$ at high pressures is similar to that at ambient pressure and 470 K,[33] exhibiting two broad peaks centered at 2.5−2.8 $Å^{-1}$ and 4.7−5.4 $Å^{-1}$, respectively. The first peak of $s(q)$ is well determined experimentally with its peak position close to the those of bcc-Li (110) and fcc-Li (111) and increasing with compression. However, the second peak of $s(q)$ is only weakly constrained. As shown in Figure 2, this is due to the uncertainty introduced by the subtraction procedures in removing the sharp features, which in turn introduces large errors in the estimated intensity. So the determined structure factors may contain large uncertainties at high-q region (q > ~4 $Å^{-1}$), leaving a limited q-range unsuitable for obtaining real-space functions. Therefore, we focus our analysis based on the first peak of $s(q)$.

https://dx.doi.org/10.1021/acs.jpcb.0c05324
J. Phys. Chem. B 2020, 124, 7258−7262

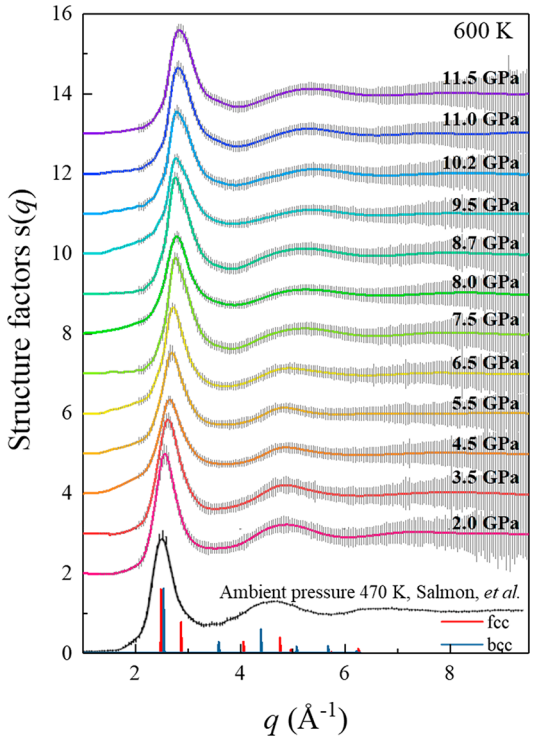

Figure 2. Obtained structure factors $s(q)$ of liquid Li at 600 ± 30 K compared with the data at ambient pressure and 470 K.[33] Ticks at the bottom indicate diffraction peak positions of the crystalline Li phases, that is, bcc-Li (blue) and fcc-Li (red).

Figure 3 shows the first peak position of $s(q)$ (q_1) as a function of pressure, along with the extrapolated positions of

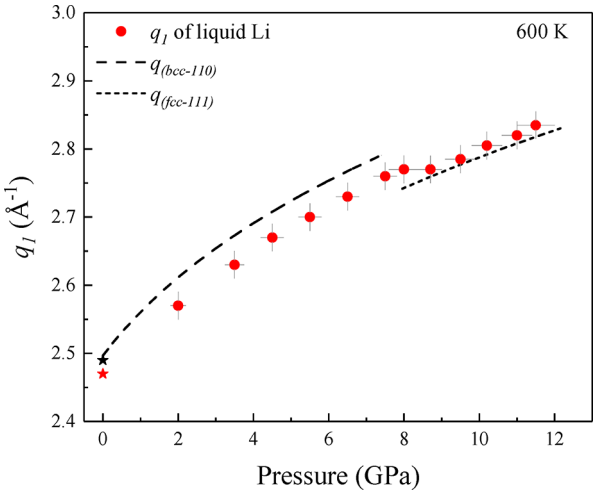

Figure 3. Determination of the q_1 position of liquid Li (red circles) as a function of pressure. The dashed lines are calculated by the equation of state for bcc-Li[39] and fcc-Li[40] and then extrapolated to 600 K with consideration of thermal expansion. The black star is the experimental q_1 value of liquid Li at ambient pressure and 453 K;[32] the red star is the corrected q_1 at 600 K.

bcc-Li [$q_{(bcc\text{-}110)}$] and fcc-Li [$q_{(fcc\text{-}111)}$] at 600 K. The extrapolated $q_{(hkl)}$ (dashed lines) of solid phases is calculated by using the equations of state for bcc-Li[39] and fcc-Li,[40] respectively. Meanwhile, a thermal expansion coefficient (α) of Li at ambient pressure and room temperature[41] is used in the estimation. The q_1 value of 2.47 Å^{-1} at ambient pressure has been corrected from 453[32] to 600 K, assuming α of 4.6 × 10^{-5}/K, which is found to be smaller than that of $q_{(bcc\text{-}110)}$ at ambient pressure, as shown in Figure 3. Under compression, our data show that the q_1 value increases gradually with increasing pressure until 7.5 GPa. The trend of the q_1 change is similar to $q_{(bcc\text{-}110)}$. Above 7.5 GPa, the q_1 value remains nearly constant around 2.77 Å^{-1} from 7.5 to 8.7 GPa until it coincides with the $q_{(fcc\text{-}111)}$ curve. We interpret the q_1 slope change in this narrow pressure range as a structural change from bcc-like local ordering to fcc-like ordering. Eventually, the fcc-like local ordering becomes dominant at pressure above 8.7 GPa. A similar trend of the q_1 change which was considered as a structural change from bcc-like to fcc-like local ordering has also been observed in liquid-K at about 5 GPa[24] and liquid-Na at 40 GPa.[42]

In solid Li, the bcc−fcc transition occurs near 9 GPa[19] at temperatures close to melting. In liquid Li, however, our data suggest that the local ordering in liquid Li may suddenly change from bcc-like to fcc-like between 7.5 and 8.7 GPa. At pressures above 8.7 GPa, the liquid structure is likely dominated by the fcc-like local ordering. Therefore, the structural changes from bcc-like to fcc-like in liquid Li occur at pressures below the solid bcc−fcc transition pressure. The structural changes in liquid Li should affect the shape of the melting curve.[23] As shown in Figure 4, the melting curve of Li

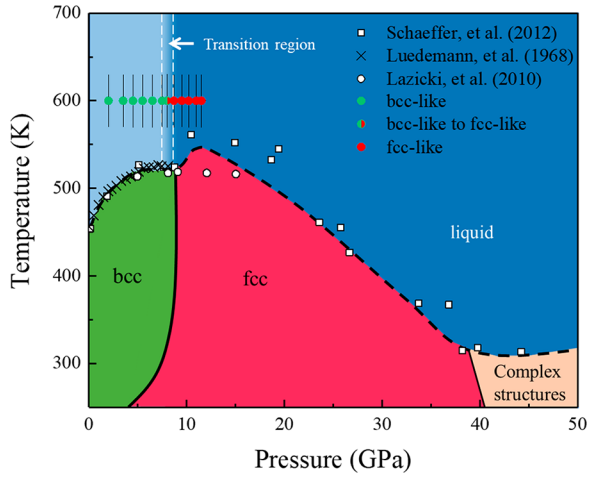

Figure 4. Experimental conditions of this study in the phase diagram of lithium. Solid colored symbols show the experimental points of this work; green and red indicate the bcc-like and fcc-like liquid structure, respectively. Crosses and open symbols are melting points from previous studies.[17,19,21] The graded blue area from 7.5 to 8.7 GPa indicates the bcc-like to fcc-like transition region of liquid Na.

displays a complex pattern.[17,19,21] In the pressure range of this study, the melting curve displays a positive slope up to ∼7 GPa and then shows a flattening melting curve up to ∼9 GPa in the bcc-Li stability field. At pressures above the bcc−fcc-liquid triple point, the results from the differential thermal analysis show a plateau in the melting curve until ∼15 GPa.[17] However, an abrupt increase of the melting temperature is observed at pressures above the triple point in studies based on simulations[30] and electrical resistivity measurements.[19] The positive slope melting curve of bcc-Li below 7 GPa can be understood in terms of the Clausius−Clapeyron relation that the entropy change and the specific volume change are positive

https://dx.doi.org/10.1021/acs.jpcb.0c05324
J. Phys. Chem. B 2020, 124, 7258−7262

at a given pressure in this pressure range.[23] The "flat" melting curve between 7 and 9 GPa, still with the underlying solid phase being bcc-Li, may be related to the bcc-like to the denser fcc-like liquid structural change that occurred at 7.5 to 8.7 GPa, as indicated by the plateau of q_1 with pressure (Figure 3). This melting curve behavior in the bcc-Li stability field is generally similar to those of other alkali metals, such as Na,[43] K,[24] Rb,[44] and Cs.[27,29] The structural changes in the corresponding alkali liquids with the structural change from bcc-like to fcc-like local ordering is the main cause of the large slope reductions and even negative slopes in the melting curves of Na,[42] K,[24] and Cs.[27,28] At pressures above the triple point, our data show no significant changes in liquid structure in the pressure range of this study. Because fcc-like local ordering becomes dominant at this pressure range, the relative volume change V/V_0 (where V_0 and V are the volumes at ambient pressure and at a given high pressure, respectively) of the liquid over 8.7 GPa may be estimated by the ratios of q_0/q (where q_0 and q are the first peak positions of fcc-Li at ambient pressure and at a given high pressure, respectively). Fitting the obtained V/V_0 data with the second order Birch−Murnaghan equation of state, we obtain a bulk modulus of 9.9 GPa for liquid Li in the pressure range of 8.7−11.5 GPa which is close to 10.43 GPa for solid fcc-Li. Thus, at pressures above the triple point the melting curve is reflected by the equilibrium between the fcc-like liquid and the fcc-structured solid. Because of the transition in solid from the bcc phase to the denser fcc phase, our structural data would support an increase of the melting curve at pressures above the bcc−fcc-liquid triple point. Similar increases in the melting curves have also been observed in K,[24,44] Rb,[44] and Cs[44] at pressures above the triple points.

A maximum in the melting curve is observed at around 11 GPa in the stability field of fcc-Li.[19] Previous theoretical studies[30,31] have suggested that this maximum is caused by different compressibility of the solid and the liquid with the liquid possessing a more anisotropic low-symmetry local structure associated with the electronic changes. In all four of the data sets collected above 9 GPa, there appears to be a weak hump around 3.6 $Å^{-1}$ in the high-q side of the first peak (Figure S4), which might suggest an appearance of the anisotropic low-symmetry local ordering. However, we consider that the signal-to-noise ratios for the hump are insufficient to make any conclusions. We present the raw data here to stimulate further studies on the low-symmetry liquid Li at higher pressure.

4. CONCLUSIONS

We have experimentally determined the structure factor $s(q)$ of liquid Li under high pressures up to 11.5 GPa along an isothermal path at 600 ± 30 K. The first peak position in $s(q)$ with compression is found to display an obvious slope change. Similar to other alkali liquid metals (Na, K, Cs), the slope change is assigned as a structural change from bcc-like to fcc-like local ordering in liquid Li between 7.5 to 8.7 GPa. At pressures above 8.7 GPa, fcc-like liquid becomes dominant up to the highest pressure of 11.5 GPa in this study. The structural change from bcc-like to fcc-like local ordering in the liquid occurs at lower pressures than the solid bcc−fcc transition pressure. The obtained structural information in liquid Li reasonably explains the slope changes in the melting curve of bcc-Li.

■ ASSOCIATED CONTENT

Supporting Information

The Supporting Information is available free of charge at https://pubs.acs.org/doi/10.1021/acs.jpcb.0c05324.

Raw EDXD data (PDF)

■ AUTHOR INFORMATION

Corresponding Author

Guoyin Shen − *High Pressure Collaborative Access Team, X-ray Science Division, Argonne National Laboratory, Argonne, Illinois 60439, United States;* orcid.org/0000-0001-5146-1147; Email: gyshen@anl.gov

Authors

Yu Shu − *High Pressure Collaborative Access Team, X-ray Science Division, Argonne National Laboratory, Argonne, Illinois 60439, United States;* orcid.org/0000-0002-0903-435X

Yoshio Kono − *Geodynamics Research Center, Ehime University, Ehime 790-8577, Japan*

Itaru Ohira − *Geodynamics Research Center, Ehime University, Ehime 790-8577, Japan; Geophysical Laboratory, Carnegie Institution of Washington, Washington, DC 20015, United States*

Rostislav Hrubiak − *High Pressure Collaborative Access Team, X-ray Science Division, Argonne National Laboratory, Argonne, Illinois 60439, United States*

Curtis Kenney-Benson − *High Pressure Collaborative Access Team, X-ray Science Division, Argonne National Laboratory, Argonne, Illinois 60439, United States*

Maddury Somayazulu − *High Pressure Collaborative Access Team, X-ray Science Division, Argonne National Laboratory, Argonne, Illinois 60439, United States*

Nenad Velisavljevic − *High Pressure Collaborative Access Team, X-ray Science Division, Argonne National Laboratory, Argonne, Illinois 60439, United States; Physics Division, Lawrence Livermore National Laboratory, Livermore, California 94550, United States*

Complete contact information is available at: https://pubs.acs.org/10.1021/acs.jpcb.0c05324

Notes

The authors declare no competing financial interest.

■ ACKNOWLEDGMENTS

Y.K. and G.S. acknowledge the support by the National Science Foundation under Award No. EAR-1722495. I.O. acknowledges the Japanese Society for the Promotion of Science (JSPS) for JSPS Overseas Research Fellowships. High Pressure Collaborative Access Team operations are supported by DOENNSA's Office of Experimental Sciences. The Advanced Photon Source is a U.S. DOE Office of Science User Facility operated for the DOE Office of Science by Argonne National Laboratory under Contract No. DE-AC02-06CH11357.

■ REFERENCES

(1) Olinger, B.; Shaner, J. Lithium, Compression and High-Pressure Structure. *Science* **1983**, *219*, 1071−1072.

(2) Neaton, J.; Ashcroft, N. Pairing in Dense Lithium. *Nature* **1999**, *400*, 141−144.

(3) Hanfland, M.; Syassen, K.; Christensen, N.; Novikov, D. New High-Pressure Phases of Lithium. *Nature* **2000**, *408*, 174−178.
(4) Lv, J.; Wang, Y.; Zhu, L.; Ma, Y. Predicted Novel High-Pressure Phases of Lithium. *Phys. Rev. Lett.* **2011**, *106*, 015503.
(5) Gorelli, F.; Elatresh, S.; Guillaume, C.; Marqués, M.; Ackland, G.; Santoro, M.; Bonev, S.; Gregoryanz, E. Lattice Dynamics of Dense Lithium. *Phys. Rev. Lett.* **2012**, *108*, 055501.
(6) Matsuoka, T.; Shimizu, K. Direct Observation of a Pressure-Induced Metal-to-Semiconductor Transition in Lithium. *Nature* **2009**, *458*, 186−189.
(7) Naumov, I. I.; Hemley, R. J. Origin of Transitions between Metallic and Insulating States in Simple Metals. *Phys. Rev. Lett.* **2015**, *114*, 156403.
(8) Miao, M. s.; Hoffmann, R.; Botana, J.; Naumov, I. I.; Hemley, R. J. Quasimolecules in Compressed Lithium. *Angew. Chem.* **2017**, *129*, 992−995.
(9) Shimizu, K.; Ishikawa, H.; Takao, D.; Yagi, T.; Amaya, K. Superconductivity in Compressed Lithium at 20 K. *Nature* **2002**, *419*, 597−599.
(10) Tuoriniemi, J.; Juntunen-Nurmilaukas, K.; Uusvuori, J.; Pentti, E.; Salmela, A.; Sebedash, A. Superconductivity in Lithium Below 0.4 Millikelvin at Ambient Pressure. *Nature* **2007**, *447*, 187−189.
(11) Ma, Y.; Eremets, M.; Oganov, A. R.; Xie, Y.; Trojan, I.; Medvedev, S.; Lyakhov, A. O.; Valle, M.; Prakapenka, V. Transparent Dense Sodium. *Nature* **2009**, *458*, 182−185.
(12) Gregoryanz, E.; Lundegaard, L. F.; McMahon, M. I.; Guillaume, C.; Nelmes, R. J.; Mezouar, M. Structural Diversity of Sodium. *Science* **2008**, *320*, 1054−1057.
(13) McMahon, M.; Gregoryanz, E.; Lundegaard, L.; Loa, I.; Guillaume, C.; Nelmes, R.; Kleppe, A.; Amboage, M.; Wilhelm, H.; Jephcoat, A. Structure of Sodium above 100 GPa by Single-Crystal X-Ray Diffraction. *Proc. Natl. Acad. Sci. U. S. A.* **2007**, *104*, 17297−17299.
(14) Lundegaard, L.; Marqués, M.; Stinton, G.; Ackland, G.; Nelmes, R.; McMahon, M. Observation of the O P 8 Crystal Structure in Potassium at High Pressure. *Phys. Rev. B: Condens. Matter Mater. Phys.* **2009**, *80*, 020101.
(15) Schwarz, U.; Grzechnik, A.; Syassen, K.; Loa, I.; Hanfland, M. Rubidium-IV: A High Pressure Phase with Complex Crystal Structure. *Phys. Rev. Lett.* **1999**, *83*, 4085−4088.
(16) Schwarz, U.; Takemura, K.; Hanfland, M.; Syassen, K. Crystal Structure of Cesium-V. *Phys. Rev. Lett.* **1998**, *81*, 2711−2714.
(17) Lazicki, A.; Fei, Y.; Hemley, R. J. High-Pressure Differential Thermal Analysis Measurements of the Melting Curve of Lithium. *Solid State Commun.* **2010**, *150*, 625−627.
(18) Guillaume, C. L.; Gregoryanz, E.; Degtyareva, O.; McMahon, M. I.; Hanfland, M.; Evans, S.; Guthrie, M.; Sinogeikin, S. V.; Mao, H. Cold Melting and Solid Structures of Dense Lithium. *Nat. Phys.* **2011**, *7*, 211−214.
(19) Schaeffer, A. M. J.; Talmadge, W. B.; Temple, S. R.; Deemyad, S. High Pressure Melting of Lithium. *Phys. Rev. Lett.* **2012**, *109*, 185702.
(20) Frost, M.; Kim, J. B.; McBride, E. E.; Peterson, J. R.; Smith, J. S.; Sun, P.; Glenzer, S. H. High-Pressure Melt Curve and Phase Diagram of Lithium. *Phys. Rev. Lett.* **2019**, *123*, 065701.
(21) Luedemann, H.; Kennedy, G. Melting Curves of Lithium, Sodium, Potassium, and Rubidium to 80 Kilobars. *J. Geophys. Res.* **1968**, *73*, 2795−2805.
(22) Tanaka, H. General View of a Liquid-Liquid Phase Transition. *Phys. Rev. E: Stat. Phys., Plasmas, Fluids, Relat. Interdiscip. Top.* **2000**, *62*, 6968.
(23) Makov, G.; Yahel, E. Liquid-Liquid Phase Transformations and the Shape of the Melting Curve. *J. Chem. Phys.* **2011**, *134*, 204507.
(24) Narygina, O.; McBride, E.; Stinton, G.; McMahon, M. Melting Curve of Potassium to 22 GPa. *Phys. Rev. B: Condens. Matter Mater. Phys.* **2011**, *84*, 054111.
(25) Tsujia, K.; Katayama, Y.; Morimoto, Y.; Shimomura, O. Structure of Liquid Rubidium under High Pressure. *J. Non-Cryst. Solids* **1996**, *205*, 295−298.
(26) Gorelli, F. A.; De Panfilis, S.; Bryk, T.; Ulivi, L.; Garbarino, G.; Parisiades, P.; Santoro, M. Simple-to-Complex Transformation in Liquid Rubidium. *J. Phys. Chem. Lett.* **2018**, *9*, 2909−2913.
(27) Falconi, S.; Lundegaard, L. F.; Hejny, C.; McMahon, M. I. X-Ray Diffraction Study of Liquid Cs up to 9.8 GPa. *Phys. Rev. Lett.* **2005**, *94*, 125507.
(28) Tsuji, K.; Yaoita, K.; Imai, M.; Mitamura, T.; Kikegawa, T.; Shimomura, O.; Endo, H. Pressure-Induced Structural Change of Liquid Cesium. *J. Non-Cryst. Solids* **1990**, *117*, 72−75.
(29) Falconi, S.; Lundegaard, L. F.; Hejny, C.; McMahon, M. X-Ray Diffraction Study of Liquid Cs up to 9.8 GPa. *Phys. Rev. Lett.* **2005**, *94*, 125507.
(30) Tamblyn, I.; Raty, J.-Y.; Bonev, S. A. Tetrahedral Clustering in Molten Lithium under Pressure. *Phys. Rev. Lett.* **2008**, *101*, 075703.
(31) Yang, J.; Tse, J. S; Iitaka, T. First-Principles Studies of Liquid Lithium under Pressure. *J. Phys.: Condens. Matter* **2010**, *22*, 095503.
(32) Gingrich, N.; Heaton, L. Structure of Alkali Metals in the Liquid State. *J. Chem. Phys.* **1961**, *34*, 873−878.
(33) Salmon, P. S.; Petri, I.; de Jong, P. H.; Verkerk, P.; Fischer, H. E.; Howells, W. S. Structure of Liquid Lithium. *J. Phys.: Condens. Matter* **2004**, *16*, 195−222.
(34) Kono, Y.; Park, C.; Kenney-Benson, C.; Shen, G.; Wang, Y. Toward Comprehensive Studies of Liquids at High Pressures and High Temperatures: Combined Structure, Elastic Wave Velocity, and Viscosity Measurements in the Paris−Edinburgh Cell. *Phys. Earth Planet. Inter.* **2014**, *228*, 269−280.
(35) Kono, Y.; Irifune, T.; Higo, Y.; Inoue, T.; Barnhoorn, A. P- V-T Relation of Mgo Derived by Simultaneous Elastic Wave Velocity and in Situ X-Ray Measurements: A New Pressure Scale for the Mantle Transition Region. *Phys. Earth Planet. Inter.* **2010**, *183*, 196−211.
(36) Liu, J.; Dubrovinsky, L.; Boffa Ballaran, T.; Crichton, W. Equation of State and Thermal Expansivity of Lif and Naf. *High Pressure Res.* **2007**, *27*, 483−489.
(37) Tsuji, K.; Yaoita, K.; Imai, M.; Shimomura, O.; Kikegawa, T. Measurements of X-Ray Diffraction for Liquid Metals under High Pressure. *Rev. Sci. Instrum.* **1989**, *60*, 2425−2428.
(38) Katayama, Y.; Tsuji, K. X-Ray Structural Studies on Elemental Liquids under High Pressures. *J. Phys.: Condens. Matter* **2003**, *15*, 6085−6103.
(39) Hanfland, M.; Loa, I.; Syassen, K.; Schwarz, U.; Takemura, K. Equation of State of Lithium to 21 GPa. *Solid State Commun.* **1999**, *112*, 123−127.
(40) Frost, M.; Levitan, A. L.; Sun, P.; Glenzer, S. Equation of State and Electron Localisation in Fcc Lithium. *J. Appl. Phys.* **2018**, *123*, 065901.
(41) Pearson, W. Thermal Expansion of Lithium, 77° to 300° K. *Can. J. Phys.* **1954**, *32*, 708−713.
(42) Raty, J.-Y.; Schwegler, E.; Bonev, S. A. Electronic and Structural Transitions in Dense Liquid Sodium. *Nature* **2007**, *449*, 448−451.
(43) Gregoryanz, E.; Degtyareva, O.; Somayazulu, M.; Hemley, R. J.; Mao, H.-k. Melting of Dense Sodium. *Phys. Rev. Lett.* **2005**, *94*, 185502.
(44) Boehler, R.; Zha, C.-S. Systematics in the Melting Behavior of the Alkali Metals from Dac Measurements. *Physica B+C* **1986**, *139-140*, 233−236.

https://dx.doi.org/10.1021/acs.jpcb.0c05324
J. Phys. Chem. B 2020, 124, 7258−7262